Available online at www.pelagiaresearchlibrary.com

Pelagia Research Library

Advances in Applied Science Research, 2012, 3 (5):2672-2678

Pelagia Research Library

ISSN: 0976-8610
CODEN (USA): AASRFC

Structural and Electrical properties of M-type Nanocrystalline Aluminium substituted Calcium Hexaferrites

Sanjay R. Gawali[a*], Kishor G. Rewatkar[b] and Vivek M. Nanoti[c]

[a]*Department Physics, Dr. Ambedkar College, Chandrapur, Maharashtra State, India (442401)*
[b]*Department of Physics, Dr. Ambedkar College, Dikshabhumi, Nagpur, Maharashtra State, India (440010)*
[c]*Priyadarshini College of Engineering, Nagpur, Maharashtra State, India (440019)*

ABSTRACT

M-type calcium ferrites with substitution of Fe^{3+} by Al^{3+} were prepared by sol-gel auto-combustion technique by blending nitrates as oxidants accompanied with fuels like urea as reducing agents. The powders were characterized using XRD and TEM. The XRD analysis indicated that the formation of single phase substituted M-type calcium hexaferrites. The average particle size of the powders were close to 94 nm. The electrical conductivity of the synthesized samples was carried out by a four – probe method in the same temperature range i.e. 300 K – 873 K. The value of ln(σ) of the samples decreases almost linearly with increasing reciprocal temperature upto transition temperature. The DC electrical resistivity of the samples at room temperature was also increases with increase in the concentration of Al^{3+} in the hexaferrite samples. The enhanced resistivity of the aluminium doped calcium hexaferrite is potential applicant in microwave devices. The drift mobility of samples was calculated from the electrical resistivity data.

Keywords: M-type hexagonal ferrite, Nanoparticles, Electrical conductivity, Activation energy, Drift mobility etc.

INTRODUCTION

Hexaferrites are classified into five types depending on chemical formulae and crystal structure. These include M-type ($CaFe_{12}O_{19}$), W-type ($CaMe_2Fe_{16}O_{27}$), X-type ($Ca_2Me_2Fe_{28}O_{46}$), Y-type ($Ca_2Me_2Fe_{12}O_{22}$), and Z-type ($Ca_3Me_2Fe_{24}O_{41}$). Recently, synthesis of one-dimensional nanostructure materials are one of the most exciting area in materials science due to their unique physical property and their potential applications in nanoscale devices and has received considerable attention during the past several years [1–2]. The researchers always attempt to invent new nano materials which could directly or indirectly be used with a little improvisation into the makings of advanced electronics nano gadgets [3]. The gadgets include nanomemory in nanobots, magnetic storage in set top box in satellite communication, HDTV, high-density magnetic tapes, floppy disks, high-coercivity magnetic media, analog and digital recorders, data retrievers, etc. For such electronics gadgets, magnetic material with nanoscaled particles with very special magnetic traits is the foremost requirement. M-type calcium hexaferrite $CaFe_{12}O_{19}$ has been intensively studied as a material for permanent magnets, high-density magnetic recording media and microwave devices [4–5].

In this respect, several low-temperature chemical methods were investigated for the formation of ultrafine $BaFe_{12}O_{19}$ particles. These methods comprised co-precipitation [6–7], hydrothermal [8–9], sol–gel [10–11], combustion [12,13], microemulsion [14], citrate precursor [15], glass crystallization [16], sonochemical [17] and mechano-chemical activation [18].

An ideal technique to synthesize calcium hexaferrites should include the following: facile operation, low anneal or calcine temperature, energy efficient and a short reaction time. In addition ultra fine powder particles with narrow particle size distribution, excellent chemical homogeneity and single magnetic domain are all the properties of an ideal M type calcium hexaferrites. In current research module, we tried a new technique, the sol-gel auto-combustion technique to synthesize calcium hexaferrite powders. It is in fact a particularly simple, safe and rapid process where in main advantages are high homogeneity, high purity and time saving and ultra fine powders.

MATERIALS AND METHODS

2.1. Sample preparations

The samples of M-type aluminium substituted calcium hexaferrites with formula $CaAl_xFe_{12-x}O_{19}$ (x=0,2,4) were synthesized by sol-gel auto-combustion technique. The synthesis technique involves the combustion of redox mixture, in which metal nitrates acted as an oxidizing reactant and urea as a reducing reactant. The initial composition of solution containing metal nitrates and urea were based on the total oxidizing and reducing valences of the oxidizer and the fuel using the concept using the concept of propellant chemistry [19].

The stoichiometric amounts of AR grade $Ca(NO_3)_2{\cdot}4H_2O$, $Fe(NO_3)_3{\cdot}9H_2O$, and $Al(NO_3)_3.9H_2O$ and urea $CO(NH_2)_2$, dissolved in an unionized distilled water at the temperature of 50 ^{0}C, were placed in a beaker. The beaker containing the solution was introduced into a microwave oven. Initially the solution boils and undergoes dehydration followed by decomposition with the evolution of a large volume of gases (N_2 , NH_3, and HNCO). After the solution reaches the spontaneous combustion, it begins burning and releases lots of heat, vaporizes all the solution instantly and becomes a solid burning at temperatures above 1000^{o}C. The entire combustion process which produces aluminium substituted calcium hexaferrite powder in microwave oven takes only few minutes.

2.2 Characterization

The crystalline structural analysis was performed by a Phillips X'pert Diffractometer (PW 1710) and using Cu-Kα radiation source and λ=1.5406 Å with 40 mA 45 KV. The scanning angle range was kept between 10^o to 120^o. The values of lattice constant 'a' and 'c', X-ray density ($\rho_{x\text{-}ray}$), bulk density (ρ_m), porosity (P) and the unit cell volume (V_{cell}) were calculated by using following equations.

$$\frac{1}{d^2} = \frac{4(h^2+k^2+hk)}{3a^2} + \frac{l^2}{c^2} \quad (1)$$

$$\rho_{x-ray} = \frac{2M}{N_A V_{cell}} \quad (2)$$

$$\rho_m = \frac{m}{\pi r^2 h} \quad (3)$$

$$P = 1 - \frac{\rho_m}{\rho_{x-ray}} \quad (4)$$

$$V_{cell} = 0.8666a^2c \quad (5)$$

Where, 'a' and 'c' are lattice constant, 'M' is the molar mass, 'm' the mass of pellet, 'r' radius of the pellet, 'N_A' Avogadro's number and 'V_{cell}' the unit cell volume.

The particle size of the samples was examined by a Transmission Electron Microscope (TEM) (Philips Model CM 200).

As these ferrites have very high resistivity, so the four probe method was employed to study DC electrical resistivity of the said ferrites system in the temperature range 300K to 873 K. The DC electrical resistivity of all the samples decreases with increasing temperature in accordance with Arrhenius equation

$$\rho = \rho_0 \exp\left(\frac{\Delta E}{k_B T}\right) \quad (6)$$

Where, 'k_B' is the Boltzmann constant, 'T' is temperature and 'ΔE' is the activation energy, which is the energy needed to release an electron from the ion for a jump to neighboring ion, giving rise to the electrical conductivity.

The activation energy of the aluminium substituted calcium hexaferrites have been determined from the slope of plots of ln(σ) versus temperature (1000/T) above and below the transition temperature (T_t).

The drift mobility (μ_d) of all synthesized hexaferrite samples were calculated using the relation

$$\mu_d = \frac{1}{ne\rho} \quad (7)$$

Where, 'e' is the charge on the electron, 'ρ' is the D.C. electrical resistivity at a given temperature and 'n' is the concentration of charge carriers and can be calculated from the relation

$$n = \frac{N_A \rho_m P_{Fe}}{M} \quad (8)$$

Where 'N_A' is the Avogadro's number, 'ρ_m' is the bulk density, 'M' is the molecular weight of the sample, 'P_{Fe}' is the number of iron atoms in the chemical formula.

RESULTS AND DISCUSSION

The diffraction pattern of samples were taken with Phillips X'pert Diffractometer and Cu-Kα radiation with wavelength λ = 1.5406 Å. The data was analyzed by using computer software PCPDF Win, Powder-X and Full proof Suite. By comparing the patterns with JCPDS, the phases in the different samples were determined. The XRD patterns confirm the formation of M-type single phase in hexagonal ferrites. The space group of the samples was observed to be $P6_3/mmc$
(Fig. 1).

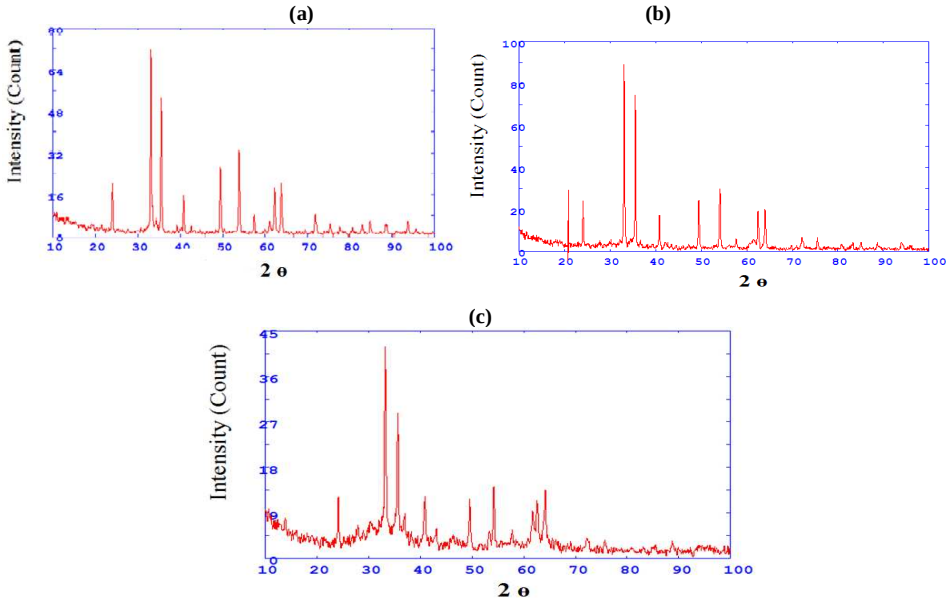

Fig.1: X-ray diffraction spectra of $CaAl_xFe_{12-x}O_{19}$: (a)x=0, (b)x=2 and x=4

Other parameters such as lattice constant (a & c), cell volume (V), X-ray density ($\rho_{x\text{-}ray}$) and bulk density (ρ_m) are enumerated in Table 1. The lattice parameter 'a' and 'c' decreases with aluminium content. This is due to relatively small ionic radius of Al^{3+} (0.53 Å) comparing to that of Fe^{3+} (0.64 Å) for six fold coordination. As a result, the cell volume of calcium ferrite decreases after doping with Al^{+3}. The results agree well with the reported one by Ounnunkad and Winotai [20] and Rewatkar [21] for Co-Al substituted calcium ferrite. Similar trend of lattice parameters and cell volume was reported by Sang Won Lee [22] in La-Zn substituted Strontium ferrite and Darokar [23] for Al and Co doped lithium hexaferrite . The X-ray density of the substituted calcium hexaferrites also decreases with the increase in the concentration of substituent as reported in Table 1. The

enhancement in X-ray density on substitution of aluminium is due to the smaller molar mass of the substituted samples. The bulk density (ρ_m) and the porosity (P) were also derived from relation 3 and 4, respectively. The X-ray density is higher than the bulk density (ρ_m) which indicates the presence of pores in the synthesized samples. The porosity increases while the bulk density decreases with increase in the Al content.

Table 1: Lattice constants a and c, cell volume (V_{cell}),, X ray density ($\rho_{x\text{-}ray}$), bulk density (ρ_m) and porosity (P) of $CaAl_xFe_{12-x}O_{19}$ samples

Substitution	Compound	a(Å)	c(Å)	V (Å) ^{3}	ρ_{xray} (g/cm^3)	ρ_m (g/cm^3)	Porosity (%)
x=0	$CaFe_{12}O_{19}$	5.8303	22.1652	652.4862	5.1619	2.8842	44.13
x=2	$CaAl_2Fe_{10}O_{19}$	5.8167	22.0932	647.3361	4.9068	2.6000	47.01
x=4	$CaAl_4Fe_8O_{19}$	5.8088	22.1045	645.9090	4.6340	2.4540	47.81

Fig 2 shows TEM photographs of aluminium substituted calcium hexaferrite. The particle size of all hexaferrite samples synthesized by sol-gel auto-combustion technique is in nano-size with an average diameter of 94 nm.

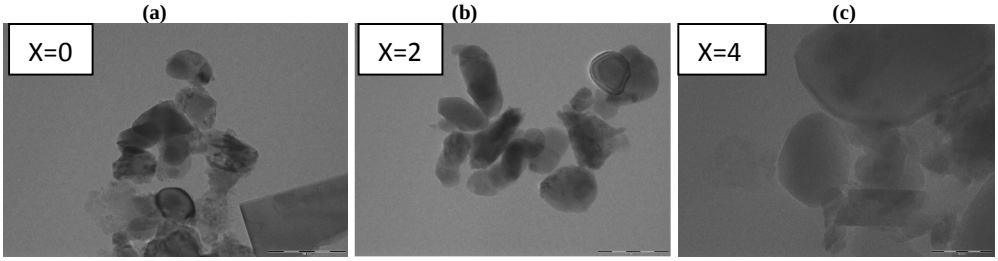

Fig.2: TEM photographs of $CaAl_xFe_{12-x}O_{19}$: (a) x=0, (b) x=2 and x=4

Fig. 3 shows the graph of electrical conductivity ln(σ) verses temperature (10^3/T) for all ferrites sample. It has be seen from the figure that the value of ln(σ) decreases almost linearly with increasing reciprocal temperature up to transition temperature (T_t), where there a slight change in slope occur in the plots. The temperature where kink is observed for the different composition of aluminium in calcium ferrites referred as transition temperature. It can be seen that the transition temperature (T_t) at which the kink is observed is in the neighborhood of its Curie temperature, hence the change in slope is attributed to magnetic phase transition. Kulkarni and Prakash [24] reported that a graph plotted for ln(σ) verses (1000/T) shows a linear behavior for $CaAl_4Fe_8O_{19}$. Went [25] observed a minute change in the slope at Curie temperature at (723K) in the plot of resistivity ln(ρ) verses temperature (10^3/T) for BaM ferrite, in contrast to the marked change in slope observed in the investigation. Table 2 shows the room temperature resistivity and activation energy of the Al-substituted samples. The activation energy of the samples in ferrimagnetic region is smaller than that in the paramagnetic region.

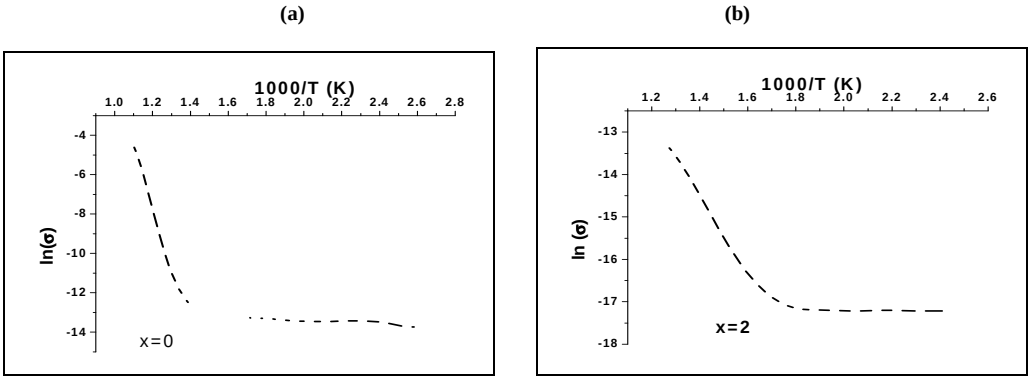

(c)

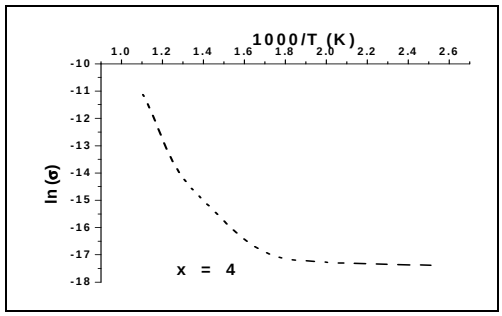

Fig.3: Variation of ln(σ) with (1000/T) of $CaAl_xFe_{12-x}O_{19}$: (a)x=0, (b)x=2 and x=4

Table 2: Electrical resistivity and activation energy in Para and Ferri magnetic regions of Al substituted Calcium ferrite

Compounds	Room Temperature Resistivity (ρ) (MΩ-cm)	Activation Energy ΔE (eV)	
		Ferri	Para
$CaFe_{12}O_{19}$	18.8	0.12	1.58
$CaAl_2Fe_{10}O_{19}$	20.9	0.35	1.51
$CaAl_4Fe_8O_{19}$	23.1	0.16	1.10

The variation in drift mobility with the temperature for aluminium substituted calcium ferrite samples shown in the Fig. 4. These samples show a curvature at a specific temperature i.e. the drift mobility increases with the increase in temperature and above the specific temperature (T_t). The drift mobility increases abruptly with increase in the temperature. The drift mobility of all the synthesized samples decreases with increasing Al concentration. The decrease in drift mobility is due to increase in resistivity by doping Al^{3+} ions. These results can be explained on the basis of the electrical resistivity data of these samples. As the electrical resistivity initially decreases with the rise in temperature below the transition temperature and above the transition temperature, the resistivity further decreases for aluminium substituted calcium hexaferrite. The initial increase in the drift mobility with increase in the temperature is due to the decrease in the electrical resistivity in the temperature range which causes to increase the mobility of the charge carriers. The increase in drift mobility above transition temperature is due to the fact that the electrical resistivity further decreases above this temperature and as a result the mobility of charge carrier increases rapidly. The values of drift mobility of the sample with temperature are in agreement with that obtained by M. Javed Iqbal and M. Naeem Ashiq [26] for Sr-hexaferrite nanomaterials.

(a) **(b)**

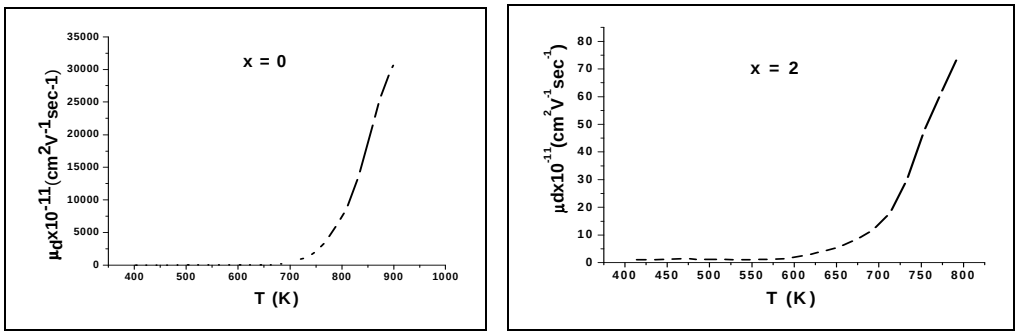

(c)

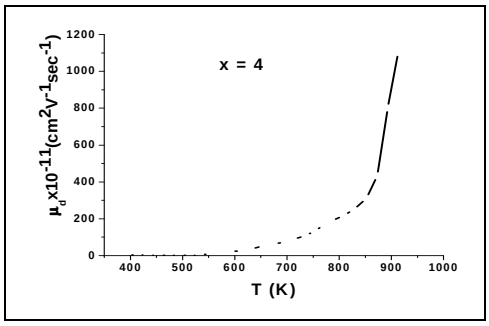

Fig. 4: Variation of drift mobility (μ_d) with temperature (T) of $CaAl_xFe_{12-x}O_{19}$: (a) x=0, (b) x=2 and x=4

CONCLUSION

Single-phase M-type aluminium-substituted calcium hexaferrite samples were synthesized by the sol-gel auto-combustion

technique. The X-ray diffraction studies confirm the formation of M type hexaferrites and the 'a' and 'c' values of the sample supports this confirmation. Structural studies have confirmed the space group of samples to be $P6_3/mmc$. The dc electrical resistivity of all the samples showed a gradual increase in the magnitude with increase in the content of Al at room temperature. This is attributed to the fact that the substituted ions localized Fe^{2+} ions and this localization induces Verwey-de Boer hopping mechanism between Fe^{2+} and Fe^{3+} ions. The increase in DC electrical resistivity suggests that the synthesized materials can be used for applications in microwave devices.

The electrical conductivity of all the samples is found to be dependent on temperature. The activation energy for all the samples is found to be different for ferrimagnetic and paramagnetic regions. The activation energy in ferrimagnetic region is observed to be less than that in paramagnetic region. The increase in drift mobility above transition temperature is due to the abrupt increase in the mobility of charge carriers.

REFERENCES

[1] Hu J.T, Odom T.W, Lieber C.M, *Acc. Chem. Res*. **1999**, 32, 435.
[2] Kind A, Yan H.Q, Messer B, Law M, Yang P. D, *Adv. Mater*. **2002**, 14, 158.
[3] Patron L, Mindru I, Marinescu G, *Dekker Encyclopedia of Nanoscience & Nanotechnology*, second edition, March **2009**.
[4] Jacobo S. E, Domingo-pascual C, Rodriguez-clemente R, *J. Mater. Sci*. **1997**, 32, 1025.
[5] Shi P, Yoon D, Zuo X, J. Appl. Phys. **2000**, 87, 4981.
[6] Abdul Samee Fawzi, *Adv. Appl. Sci. Research*, **2011**, 2 (5), 577-589.
[7] Khot S. S, Shinde N. S, Ladgaonkar B. P, Kale B. B, Watawe S. C, *Adv. Appl. Sci. Research*, **2011**, 2 (4), 460-471.
[8] Lechevallier L, Le Breton J. M, Wang J. F, Harris I. R, *J. Magn. Magn. Mater*. **2004**, 269, 192.
[9] Mishra D, Anand S , Panda R. K, Das R. P, *Mater. Chem. Phys*. **2004**, 86, 132.
[10] He H. Y, *Advan. Natur. Appl. Sci*., **2009**, 3(2), 211.
[11] Zhong W, Ding W, Zhang N, Hong J, Yan Q, Du Y, *J. Magn. Magn. Mater*. **1997**, 168, 196.
[12] Sharma A, Modi O, Gupta G, *Adv. Appl. Sci. Research*, **2012**, 3 (4), 2151-2158.
[13] Bangale S. V, Patil D. R, Bamane S. R, *Arch. Appl. Sci. Research*, **2011**, 3 (5) 506-513.
[14] Pillai V, Kumar P, Multani M. S, Shah D. O, *Colloids Surf. A: Physicochem. Eng. Aspects* **1993**, 80, 69.
[15] Sankaranarayanan V. K, Khan D. C, *J. Magn. Magn. Mater*. **1996**, 153, 337.
[16] El-Hilo M, Pfeiffer H, O'Grady K, Schuppel W, Sinn E, Gornert P, Rosler M, Dickson D. P. E, Chantrell R. W, *J. Magn. Magn. Mater*. **1994**, 129, 339.
[17] Shafi K. V. P. M, Gedanken A, *Nanostructured Mater*. **1999**, 12, 29.
[18] Abe O, Narita M, *Solid State Ionics* **1997**, 103, 101.
[19] Jain S. R, Adiga K. C, Pai Verneker V. R, *Combust Flame* **1981**, 40, 71.

[20] Ounnunkad S, Winotai P, *J. Magn. Magn. Mater*. **2006**, 301, 292.
[21] Rewatkar K. G, Patil N. M, Gawali S. R, *Bull. Mater. Sci*. **2005**, 28(6), 585.
[22] Sang Won Lee, Sung Yong An, In-Bo Shim, Chul Sung Kim, *J. Magn. Magn. Mater*. **2005**, 290, 231.
[23] Darokar S. S, *Adv. Appl. Sci. Research*, **2012,** 3 (3) 1395-1398.
[24] Kulkarni D. K, Prakash C. S, *Bull. Mater. Sci.* **1994**, 17, 35.
[25] Went J. J, Rathenau G. W, Gorter E. W, Oosterhout G. W. V. *Philips Tech. Rev*. **1952**, 13, 194.
[26] Muhammad J. Iqbal, Muhammad N. Ashiq, Pablo Hernandez-Gomez, *J. Alloy Compd*. **2009**, 478, 736.